Supporting information for "Diesel passenger vehicle shares influenced COVID-19 changes in urban nitrogen dioxide pollution"

Gaige Hunter Kerr[1,*], Daniel L. Goldberg[1], K. Emma Knowland[2,3,#], Christoph A. Keller[2,3,#], Dolly Oladini[4], Iyad Kheirbek[5], Lucy Mahoney[4], Zifeng Lu[6], and Susan C. Anenberg[1]

[1] Department of Environmental and Occupational Health, Milken Institute School of Public Health, The George Washington University, Washington, DC, USA
[2] Universities Space Research Association (USRA)/GESTAR, Columbia, MD, USA
[3] NASA Goddard Space Flight Center (GSFC), Global Modeling and Assimilation Office (GMAO), Greenbelt, MD, USA
[4] C40 Cities, London, England, UK
[5] C40 Cities Climate Leadership Group Inc., New York, NY, USA
[6] Systems Assessment Center, Energy Systems Division, Argonne National Laboratory, Lemont, IL, USA
[#] Now at Morgan State University/GESTAR-II, Baltimore, MD, USA

E-mail: *gaigekerr@gwu.edu

Text S1: NO_2 observations

We obtain observed hourly NO_2 concentrations from 1 January 2019 to 30 June 2020 from the European Environment Agency [1]. The number of NO_2 monitors in each city considered for this study varies from 2 in Zagreb, Croatia to 126 in London, United Kingdom with an average of ∼13 monitors per city (Table S1, Figure S1). We generally choose one city per country (usually the capital or largest city) as publicly available databases on diesel shares at the subnational level do not exist to our knowledge. However, for some countries (e.g., Germany, Italy) we select two cities within a county if both cities have their own traffic trends to illustrate how different meteorology and changes in traffic impact results.

To the best of our knowledge, all monitors are regulatory-grade (not low-cost). Most regulatory monitors measure using the chemiluminescence method, which captures other reactive nitrogen species such as nitric oxide and a small fraction of nitric acid. The designation of a monitor as belonging to a particular city is determined using municipality or equivalent unit definitions from the Nomenclature of Territorial Units for Statistics, a hierarchical system for delineating administrative units in Europe.

While we primarily feature this European cohort of cities in our study due to the

need to have a range in diesel shares, we complement this cohort with four additional cities in the Americas and Oceania (Auckland, New Zealand; Mexico City, Mexico; Los Angeles, United States of America; and Santiago, Chile). These additional cites report data to C40 Cities as part of the C40 Cities network. They generally have lower diesel shares than European cities (Table S1) and specifically allow us to test whether our results are robust for cities with these small diesel shares.

Text S2: Diesel, traffic, and stay-at-home data

We rely on national-level diesel shares for the most recent year available (generally 2019) from the European Automobile Manufacturers Association and International Council on Clean Transportation [2, 3]. We focus on passenger vehicle diesel shares for two reasons. The first is that most heavy-duty vehicles, regardless of country, use diesel fuel [3] whereas there is a wide range of passenger vehicles diesel shares (Table S1). The second reason we focus on passenger vehicles is that one of the most salient impacts of the pandemic was on the passenger vehicle sector given the shift to remote work for many jobs [e.g., 4, 5]. Using national-level data assumes that diesel shares are homogeneous throughout individual countries and does not account for regional or local policies (e.g., low emission zones in city centers) that may target diesel vehicles. If more than one city from a particular country is used in our study, these cities have the same diesel shares.

We account for changes in traffic emissions on NO_2 concentrations using Apple Mobility Trends Reports [6], which provide daily traffic trends during COVID-19 relative to a baseline volume from 13 January 2020 (Figure S2). We select the highest level of granularity available for a given city. Of our 22 focus cities, 19 have traffic data aggregated to the city-level, and we use national-level data for the other three cities (Table S1). This dataset has been previously used to examine the impacts of different degrees of social distancing on COVID-19 spread [7] and air quality [8].

The timing of stay-at-home measures and lockdowns varies across and within countries, and we use the Oxford COVID-19 Government Response Tracker (OxCGRT) to provide country-specific dates of stay-at-home recommendations and requirements [9]. OxCGRT discretizes stay-at-home measures into four categories ranging from "no measures" to "required to not leave the house with minimal exceptions" (Figure S2).

Text S3: GEOS-CF

NASA's GEOS-CF v1.0 provides three-dimensional gridded historical estimates of meteorology and atmospheric composition at $0.25° \times 0.25°$ ($\sim$ 25 km) horizontal resolution globally from the surface to about 80 km for the period since 1 January 2018 [10]. This is possible because the GEOS-Chem chemical transport model [11] is fully integrated into the GEOS Earth System Model [12, 13, 14]. We obtain near-surface (lowest model level) hourly-average meteorological and atmospheric composition fields (Table S2) from GEOS-CF from 1 January 2019 to 30 June 2020 and thereafter sample

the model for the grid cell closest to the location of each air quality monitor within individual cities shown in Figure S1.

It is important to note that the meteorology and fire emissions are constrained by observations; in particular, the inclusion of fire radiative power based on MODIS from the Quick Fire Emissions Dataset [QFED; 15] informs the model of recent fires. Anthropogenic NO_x emissions are generally derived from the global Hemispheric Transport of Air Pollution inventory [HTAP; 16]. HTAP v2.2 harmonizes the complete global coverage of EDGAR with the latest-available regional inventories. GEOS-CF v1.0 incorporates the monthly HTAP v2.2 anthropogenic emissions from 2010 for all subsequent years and applies weekly and diurnal scaling factors [10]. Therefore, the model has no knowledge about COVID-19 restrictions impacting anthropogenic emissions but does have realistic meteorology and fire emissions for 2019 and 2020 and thus represents a business-as-usual scenario for the COVID-19 period [see also 17]. Full details regarding the GEOS-CF configuration and available model output are described by Keller and colleagues [17, 10] and Knowland and colleagues [18], respectively.

Text S4: Emissions inventories

We use the Greenhouse gas–Air pollution Interactions and Synergies (GAINS) model [19] to quantify NO_x emissions from light-duty vehicles. GAINS is an integrated assessment model that brings together emissions estimates from a number of global inventories and direct submissions from European Union member states. These estimates are then merged within GAINS' unified framework to estimate historic emissions of key air pollutants and greenhouse gases.

GAINS disaggregates NO_x emissions by vehicle category (e.g., light-duty vehicles, heavy-duty vehicles), unlike many publicly available gridded inventories that only include on-road transportation emissions. This capability allows us to calculate the contribution of NO_x emissions from light-duty vehicles to total anthropogenic NO_x emissions. These emissions are only available as national sums, and we use these national-level estimates for each country in our analysis. This level of granularity is consistent with our use of national-level diesel shares (Text S2). Similar to our treatment of diesel shares, cities within the same country share the same value for light-duty vehicle and total NO_x emissions.

We specifically consider two different GAINS baseline emissions scenarios: ECLIPSE (V6b CLE) and the Second Clean Air Outlook [20, 21] and average these two scenarios together to create a single estimate per city. NO_x emissions from these scenarios represent 2020 values. These 2020 emissions scenarios do not consider any impacts of the COVID-19 pandemic. While the scenarios use some common data inputs, including both indicates how different methods and assumptions within GAINS may impact the estimated contribution on light-duty vehicle emissions to total NO_x emissions.

Text S5: Data post-processing

We average observed NO_2 and modeled meteorology- and composition-related variables to daily mean values from hourly time slices beginning 0000 UTC. For each focus city, all variables taken from *in-situ* monitors or model grid cells colocated with monitors are spatially averaged to produce a "meta-site" following Ivatt and Evans [22] that represents daily observed or modeled NO_2, meteorology, and composition at the city level.

Our machine learning technique trains on data from 2019; however, the Apple Mobility Trends Reports dataset begins on 13 January 2020. To remedy this issue, we calculate mean day-of-the-week-specific traffic volumes from 13 January 2020 to 29 February 2020 to capture volumes prior to most stay-at-home measures (e.g., Figure S2) and thereafter apply these day-of-the-week-specific volumes to the period spanning 1 January 2019 to 12 January 2020. While this reconstructed time series is imperfect and may miss seasonal variations or holidays, it captures weekday-weekend patterns, which are important for urban NO_2.

Text S6: Machine learning algorithm

For each city meta-site, we use a k-fold cross validation technique to predict the time-varying bias between GEOS-CF and observed NO_2 with the following steps:

(i) Data from 1 January to 31 December 2019 are decomposed into six 2-month folds. We split the data into consecutive folds, without reshuffling, to avoid overfitting due to the autocorrelation present in the data. The first fold is reserved for validation, and we build a bias-corrected model using the remaining five folds as a training dataset. We do not include data from 2020 in the training of the bias corrector. Previous work has demonstrated that one year of data is adequate for bias-correcting an atmospheric composition model to observations [22].

(ii) We quantify model performance using a variety of metrics with the reserved (testing) fold and training folds (Figure S3).

(iii) We use the bias-corrected model derived from each fold to predict the bias for the entire measuring period (1 January 2019 - 30 June 2020).

(iv) The first three steps are repeated five times (thus, every fold of the dataset is treated as a test), resulting in a total of six bias-corrected models. We average bias-corrected NO_2 concentrations over these six folds [17, 10].

We use default parameter values, listed in Table S3, when tuning the XGBoost model. Optimizing these parameters would be computationally expensive and beyond the scope of our study, but we note that their impact on XGBoost performance been investigated in a recent study [17]. In this study, XGBoost performance was found to only marginally improve when parameter values beyond the defaults were used.

We test whether XGBoost-inferred ΔNO_2 could be a function of our choice of time periods for training data. To do so, we estimate ΔNO_2 for two additional time periods.

(i) First, we train on 2018 data and apply this model to 1 January 2019 to 30 June 2019. Since there was no unprecedented drop in NO_x emissions during early 2019, we hypothesize that this application of XGBoost will not lead to a substantial ΔNO_2 in 2019. This hypothesis indeed holds for our focus cities (Figure S4). For example, in Paris we calculated ΔNO_2 = -1.9% in January-June 2019 compared to the ∼40% decrease we found during COVID (Figure 3 in the main text).

(ii) Second, we train on data from 1 January to 30 June 2018 and 2019 and apply this model to the COVID-19 period. The rationale behind this sensitivity test is whether XGBoost could underpredict in one season and overpredict in another season during the 2019 training period used elsewhere in this study, falsely giving the impression of good performance when averaged over a year. Our hypothesis is that training XGBoost on January-June 2018 and 2019 and thereafter applying this model to the COVID-19 period will still show a substantial decrease in NO_2 during the pandemic. We find that this is the case in our focus cities (Figure S5). Using Paris again as an example, we found ΔNO_2 = -44.7% using the full 2018-2019 training period. This decrease is in reasonable agreement with the ∼40% decrease in Figure 3 in the main text.

Both these sensitivity tests speak to the ability of XGBoost to detect changes in NO_2 during the pandemic and indicate that the estimated ΔNO_2 in early 2020 was not an artifact of choices we made regarding training data for the model.

We exploit SHapley Additive exPlanations (SHAP) values to increase the interpretability of business-as-usual NO_2 concentrations. SHAP values employ game theory to explain the contribution of individual input variables in predicting the bias [23, 24, 25]. For each of the k folds in each city and for each day, SHAP values are assigned to each input variable used to generate the predicted bias between GEOS-CF and observed NO_2 representing the marginal contribution of each input variable. Variables with larger absolute SHAP values therefore have a greater influence on correcting the bias between GEOS-CF and observed NO_2. We show partial dependence plots for each input variables to XGBoost in Figure S5. Many of the input variables have a U-shaped impact on predicting the bias between observed and modeled NO_2 (Figure S5). This result means that very low and very high values of the input variables have the greatest impact on predicting the bias. Since the predicted NO_2 is the bias between a $0.25° \times 0.25°$ grid cell and a point observation, days with high or low values for variables could represent a scenario in which the modeled values of these variables in the entire grid cell substantially differ from local conditions at the monitor. For example, on days with extremely high or low traffic volumes, we might that the modeled NO_2 concentrations would have a larger degree of disagreement with observations than on days with average traffic volumes on account of the resolution of GEOS-CF (i.e., higher traffic volumes in city → elevated NO_2 concentrations at monitor compared to the

underlying grid cell → larger bias).

Since XGBoost is unable to extrapolate beyond the training range [22], it is most appropriate to consider ΔNO_2 as accounting for weekday-weekend variations in traffic but not for the plummeting traffic volumes in spring 2020. To determine whether traffic volumes from Apple Mobility Trends Reports serve as a proxy for the day of the week, we also perform a sensitivity analysis in which we recalculate ΔNO_2 using the day of the week (e.g., Monday = 0, Tuesday = 1, etc.) as an input variable rather than traffic volumes (Figure S8).

Text S7: Sensitivity to traffic dataset

Accounting for differences in traffic among cities and traffic's impact on NO_2 pollution requires spatially- and temporally resolved traffic data. Mobility datasets typically cover only specific regions or are cost prohibitive. Apple and Google have offered data on mobility trends during the pandemic, which is an important step to provide a globally consistent, open-access dataset on traffic trends. We found that Apple Mobility Trends Reports offer greater granularity than Google's COVID-19 Community Mobility Reports for our focus cities; however, three of our 22 cities lack city-specific traffic trends, and we relied on country-level data (Table S1). Apple does not provide information about the representativeness of their mobility data against the overall population. It is possible that socioeconomic factors or cellphone preferences may lead to the Apple data being representative of a certain subset of the population in a given city. Political and cultural differences across and within countries might also lead to different reactions and willingness to adhere to stay-at-home measures that may not be reflected in mobility data.

We obtained traffic counts directly from two of the focus cities (Berlin and Milan) who report their traffic data to C40 Cities and compared these counts with the Apple dataset. While these different datasets record intrinsically different quantities (number of passing vehicles at *in-situ* traffic counters versus anonymized mobile phone location data), these two datasets have demonstrably similar trends during the pandemic (Figure S12a-b). Recalculating bias-corrected ΔNO_2 with these *in-situ* traffic counts yields similar values as those calculated with the Apple dataset (Figure S12c-d).

Neither the Apple dataset or *in-situ* counts for Milan and Berlin capture information on changes in vehicle speed. NO_x emissions generally increase with vehicle speed [26], and it is possible that changes in congestion and the types of roads driven on during the pandemic (e.g., local roads versus highways) impact average vehicle speeds and therefore NO_x emissions.

City	Share of passenger diesel vehicles [%]	Number of *in-situ* monitors	Traffic	Passenger vehicle age[a] [years]
Athens, Greece	8.1[a]	4	city-level	16.0
Barcelona, Spain	58.7[a]	7	city-level	12.7
Berlin, Germany	31.7[a]	17	city-level	9.6
Budapest, Hungary	31.5[a]	5	city-level	13.5
Copenhagen, Denmark	30.9[a]	3	city-level	8.8
Helsinki, Finland	27.9[a]	3	city-level	12.2
Krakow, Poland	31.6[a]	3	city-level	14.1
London, United Kingdom	39.0[a]	126	city-level	8.0
Madrid, Spain	58.7[a]	24	city-level	12.7
Marseille, France	58.9[a]	3	city-level	10.2
Milan, Italy	44.2[a]	5	city-level	11.4
Munich, Germany	31.7[a]	4	city-level	9.6
Paris, France	58.9[a]	10	city-level	10.2
Prague, Czechia	35.9[a]	9	city-level	14.9
Rome, Italy	44.2[a]	13	city-level	11.4
Rotterdam, Netherlands	14.0[a]	8	city-level	11.0
Sofia, Bulgaria	43.1[c]	5	country-level	15.0
Stockholm, Sweden	35.5[a]	4	city-level	10.0
Vienna, Austria	55.0[a]	15	city-level	8.3
Vilnius, Lithuania	69.2[a]	4	country-level	16.8
Warsaw, Poland	31.6[a]	3	city-level	14.1
Zagreb, Croatia	52.4[a]	2	country-level	14.6
Auckland, New Zealand	8.3[b]	7[b]	city-level	–
Los Angeles, United States	0.4[b]	15[b]	city-level[d]	–
Mexico City, Mexico	0.2[b]	32[b]	city-level	–
Santiago, Chile	7.1[b]	9[b]	city-level	–

Table S1. Focus cities and information about their vehicle fleets, traffic data, and *in-situ* monitor networks. Unless otherwise indicated, *in-situ* monitors are taken from the European air quality database, AirBase, maintained by the European Environment Agency. Rows in grey denote cities outside of the European Union included in the sensitivity analysis.

[a] Data derived from European Automobile Manufacturers Association.

[b] Based on data reported by city agencies to C40 Cities.

[c] Data derived from ICCT.

[d] City-level traffic data for Los Angeles represent an average over Los Angeles and Orange counties.

Family and variables	Source
Composition: CO, NO_2, O_3, $PM_{2.5}$, SO_2	GEOS-CF
Meteorology: Eastward wind, northward wind, fractional cloud cover, surface pressure, total precipitation, air temperature, planetary boundary layer height, specific humidity, relative humidity, sea level pressure	GEOS-CF
Mobility: Traffic	Apple Mobility Trends Reports

Table S2. Input variables used in the XGBoost machine learning algorithm. All variables from GEOS-CF represent near-surface values (lowest model level; > 985 hPa).

XGBoost Parameter	Value
`booster`	`gbtree`
`eta`	`0.3`
`gamma`	`0`
`max_depth`	`6`
`min_child_weight`	`1`
`max_delta_step`	`0`
`subsample`	`1`
`colsample_bytree`, `colsample_bylevel`, `colsample_bynode`	`1`
`lambda`	`1`
`alpha`	`0`
`tree_method`	`auto`
`scale_pos_weight`	`1`
`refresh_leaf`	`1`
`process_type`	`default`

Table S3. XGBoost general and booster parameters used in this study. Values represent the default used by the open-source XGBoost software library [27].

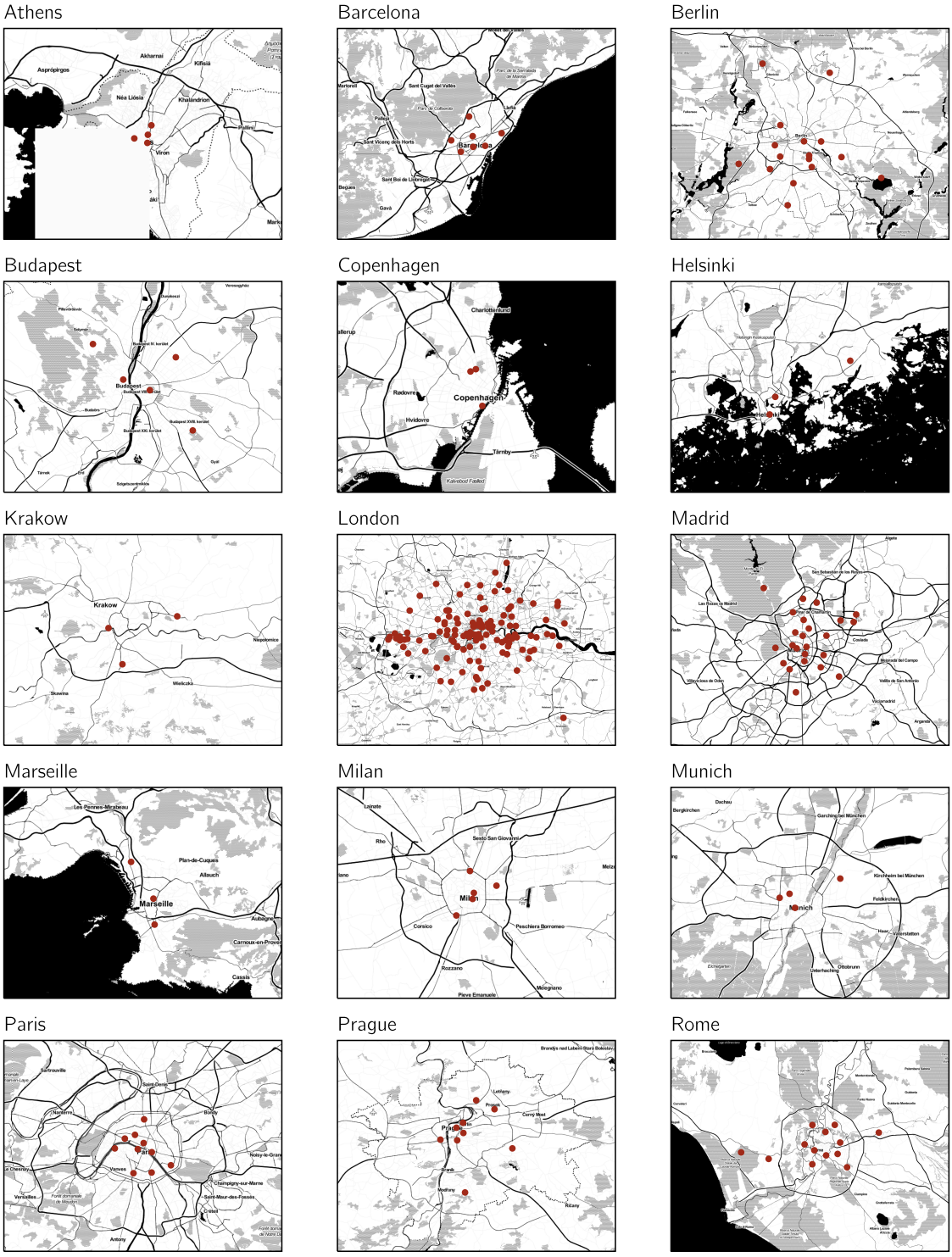

Figure S1. Location of *in-situ* NO_2 monitors in focus cities. Bodies of water are denoted in black, and grey stippling indicates city parks or other green spaces. Map tiles were created by Stamen Design (`https://stamen.com`) and include data from OpenStreetMap.

Rotterdam

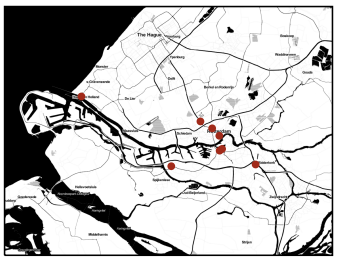

Sofia

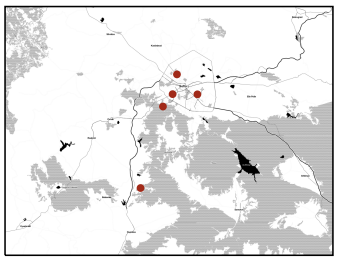

Stockholm

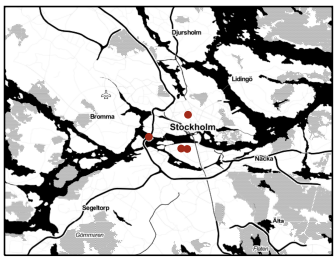

Vienna

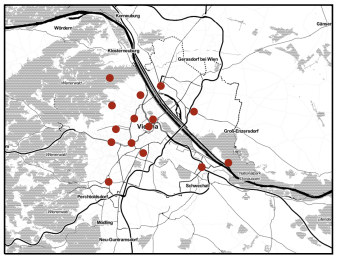

Vilnius

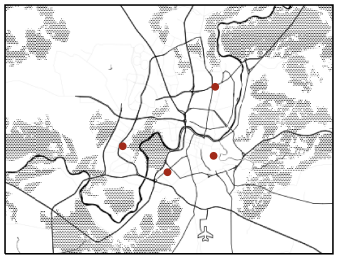

Warsaw

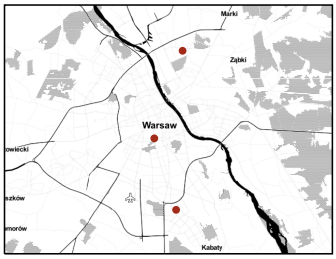

Zagreb

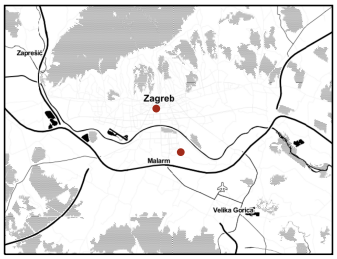

Figure S1 (Cont.).

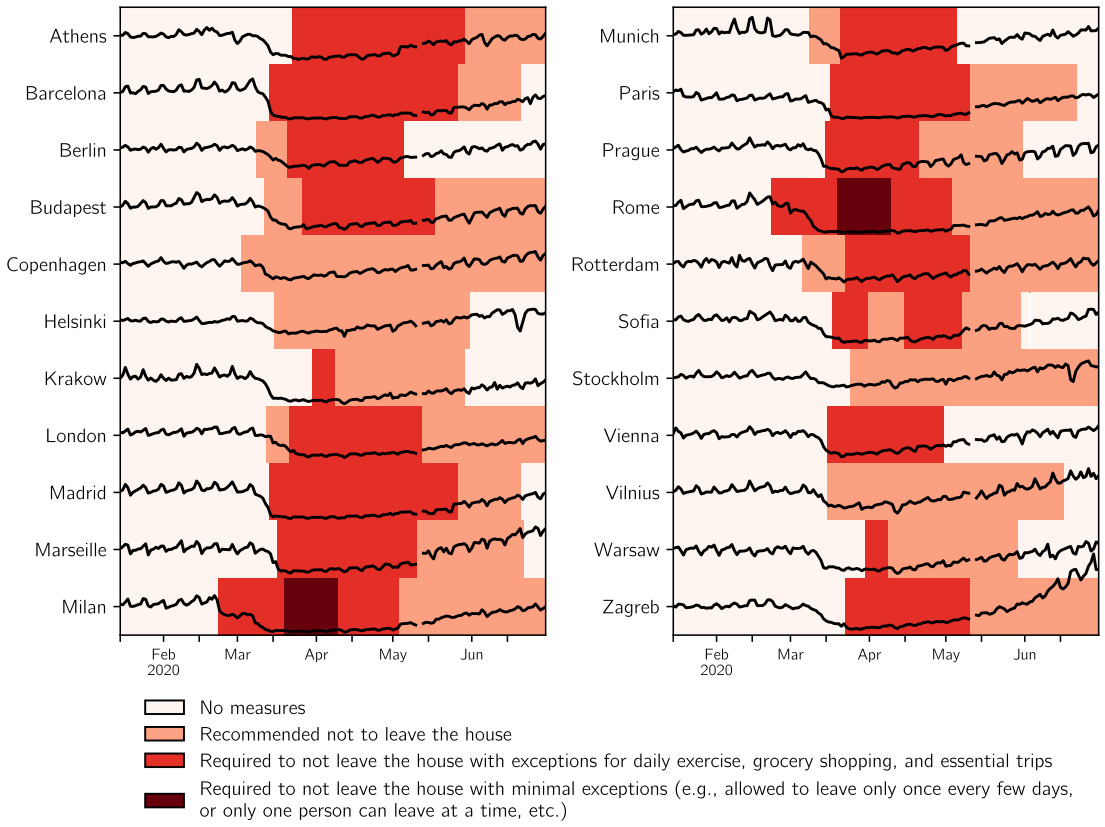

Figure S2. Focus cities' traffic patterns and stay-at-home measures. Black time series qualitatively show city- or county-specific traffic volumes from the Apple Mobility Trends Reports relative to a baseline volume on 13 January 2020. Data for 11-12 May 2020 are not available. Colors indicate national-level stay-at-home recommendations or requirements for the country containing focus cities. Note that the different stay-at-home categories may not apply to every region within a country.

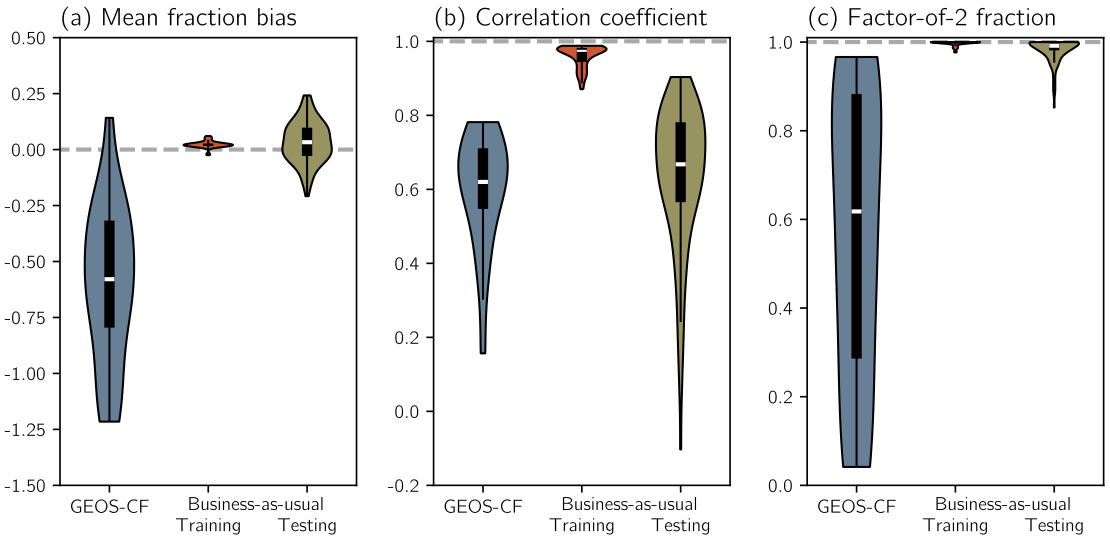

Figure S3. Evaluation metrics measuring the performance of NO_2 from GEOS-CF and the training and testing sets of the bias-corrected business-as-usual NO_2 against observed NO_2 for 2019. Violins for GEOS-CF correspond to metrics for each focus city, while violins for the training and testing sets correspond to metrics from individual folds of the k-fold cross validation for each city. The median values, first and third quartiles, and extrema are denoted by the white lines, boxes, and whiskers, respectively, if space within violins allows. Dashed grey lines indicate the value of each metric for a model that perfectly matches the observed data.

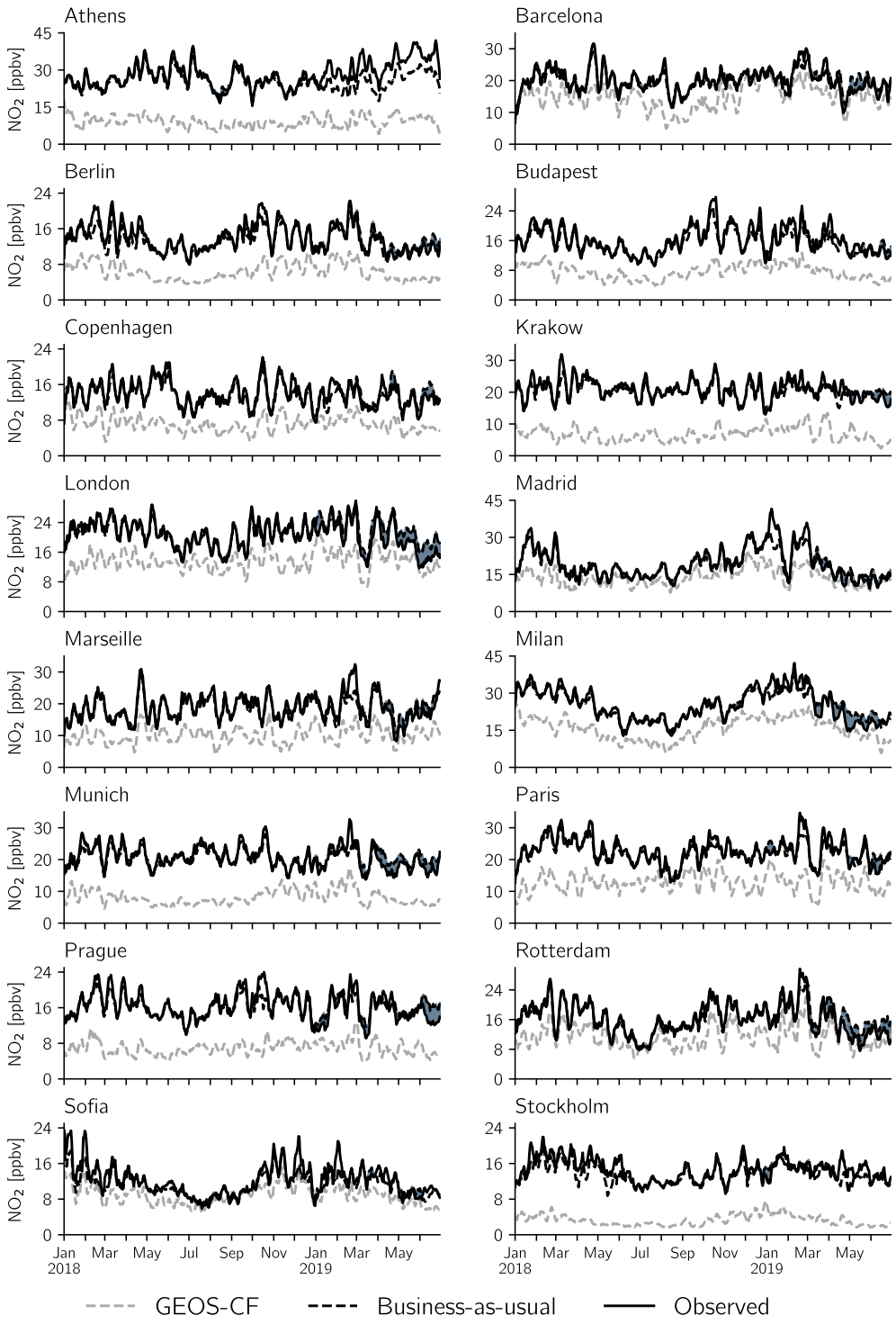

Figure S4. Sensitivity of XGBoost-inferred ΔNO_2 to training data, illustrated by training XGBoost on 2018 data and applying to 1 January 2019 to 30 June 2019. Interpretation follows Figure 2a in the main text. Rome and Helsinki do not have observations in 2018, so these cities are omitted from this analysis.

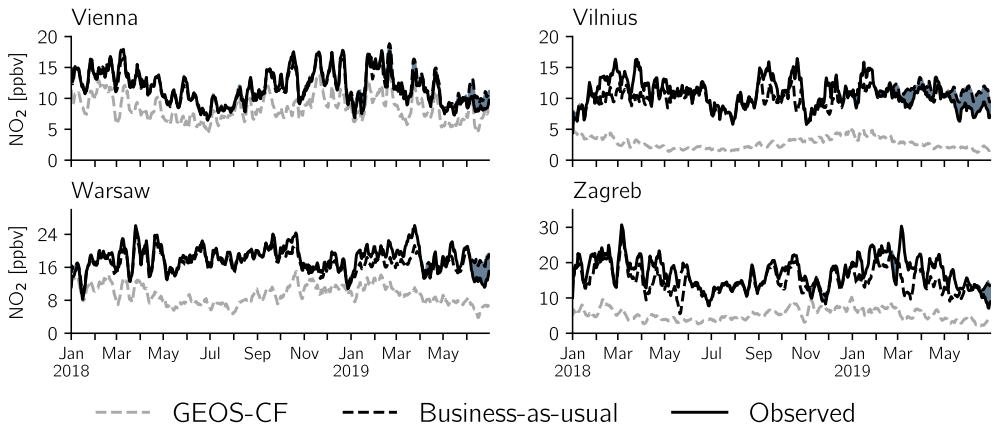

Figure S4 (Cont.).

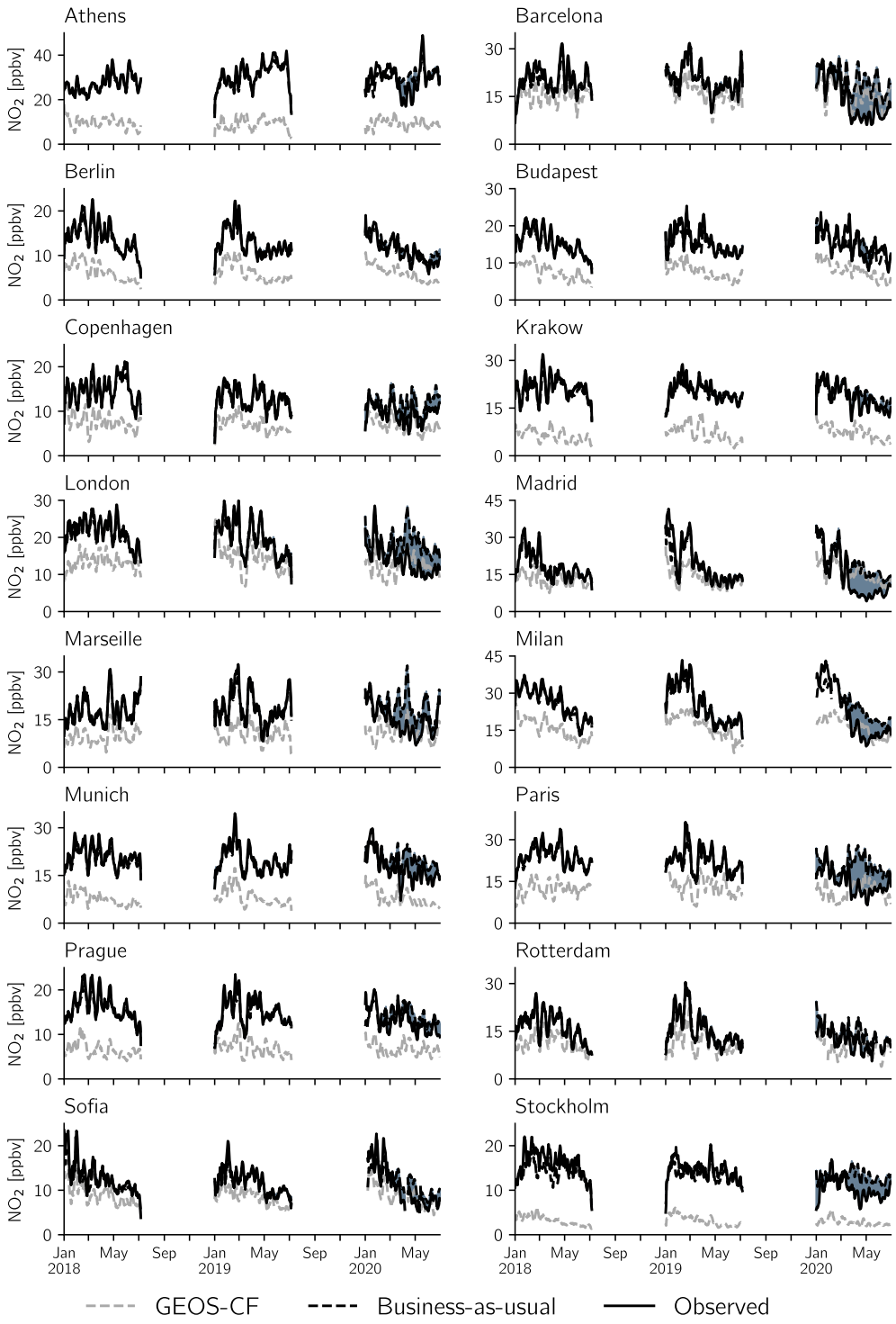

Figure S5. Sensitivity of XGBoost-inferred ΔNO_2 to training data, illustrated by training XGBoost on 1 January to 30 June 2018 and 2019 data and applying to 1 January to 30 June 2020. Interpretation follows Figure 2a in the main text. Rome and Helsinki do not have observations in 2018, so these cities are omitted from this analysis.

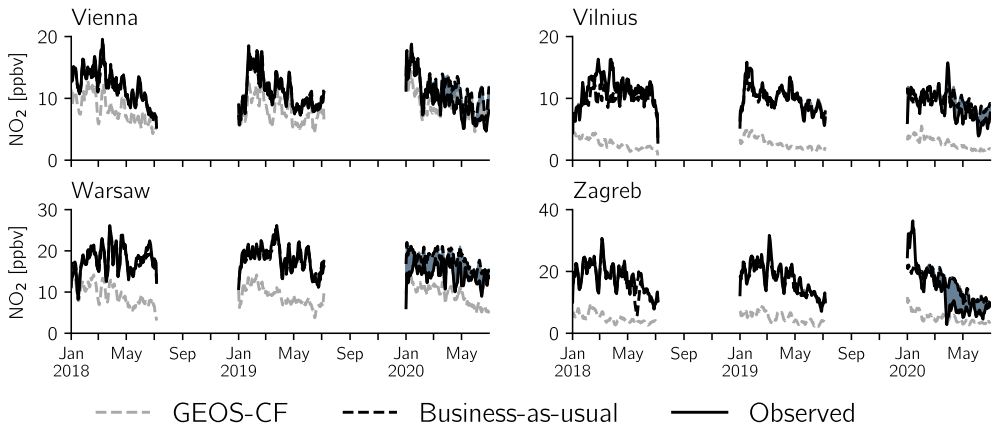

Figure S5 (Cont.).

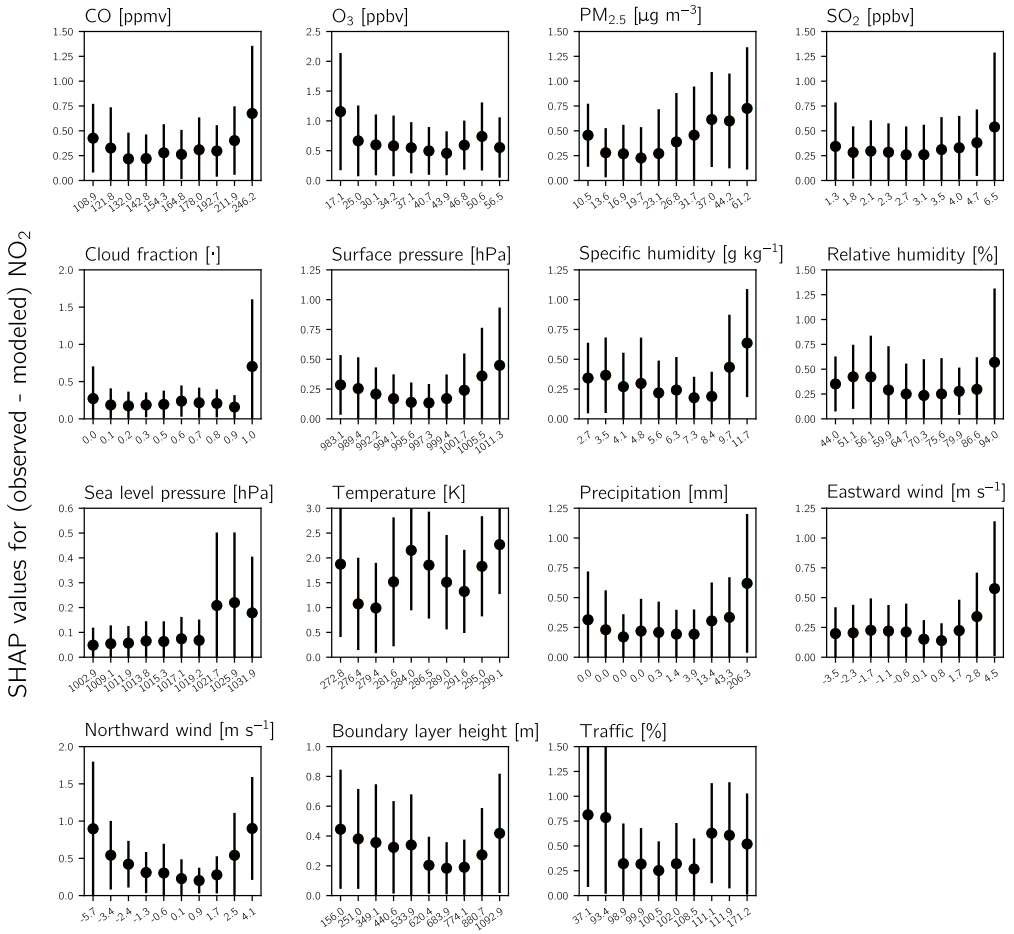

Figure S6. Partial dependence plots of predicted observation-model NO_2 bias for input variables. Input variables are discretized into decile bins, and the mean values of these bins are denoted on the horizontal axis tick labels. Scatter points represent the mean SHAP values in each decile bin, and the vertical bars show denote the standard deviation for the SHAP values.

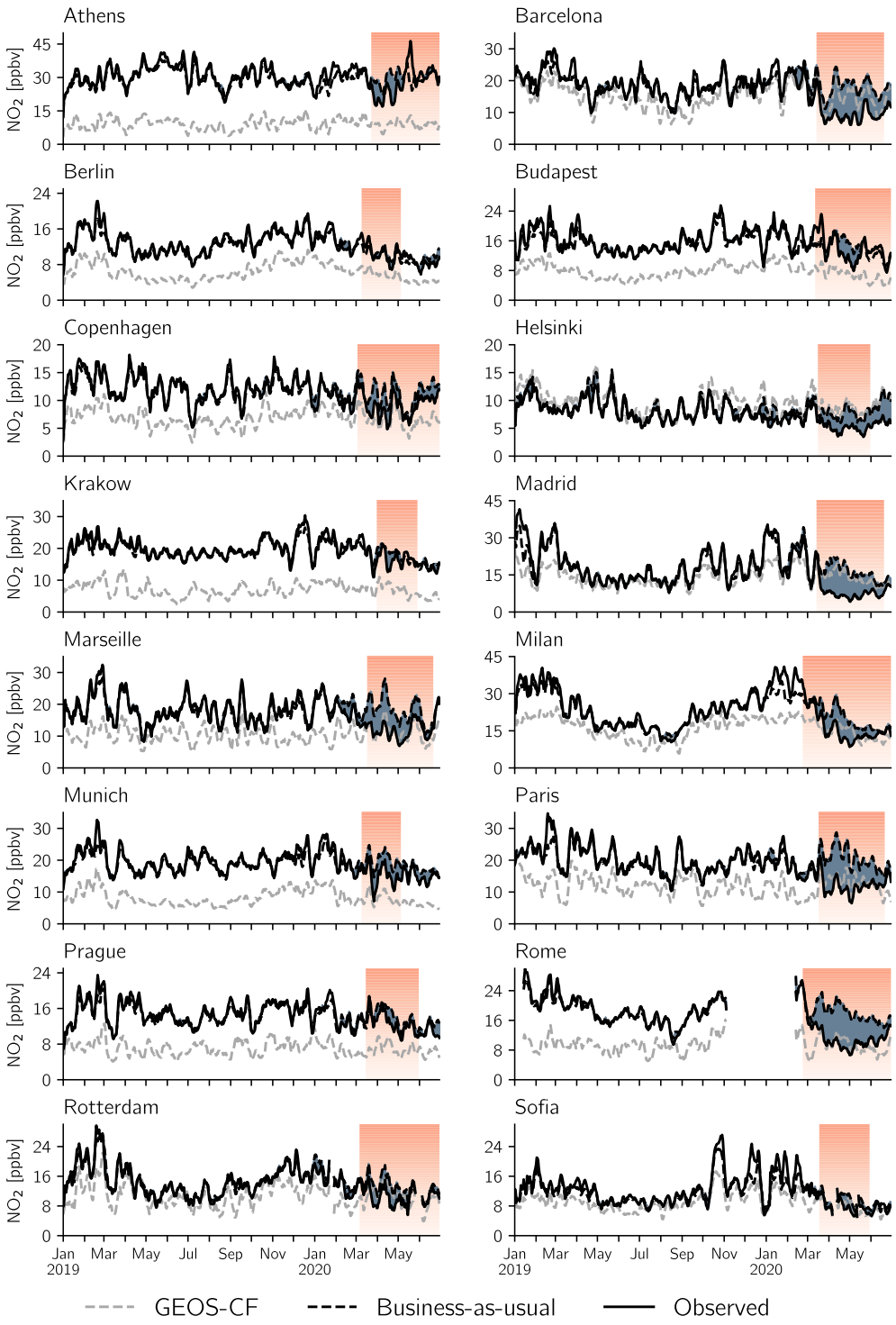

Figure S7. Same as Figure 2a in the main text but for other focus cities.

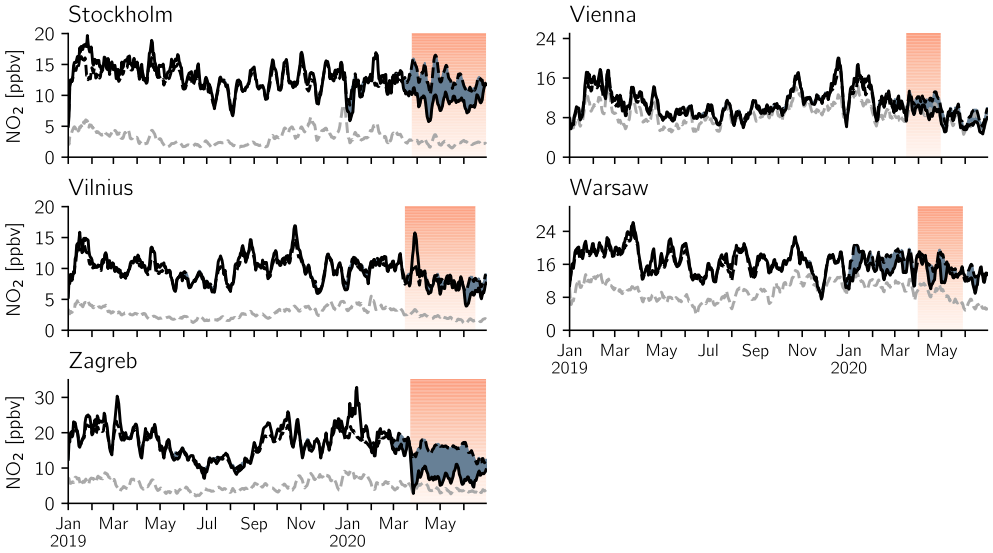

Figure S7 (Cont.).

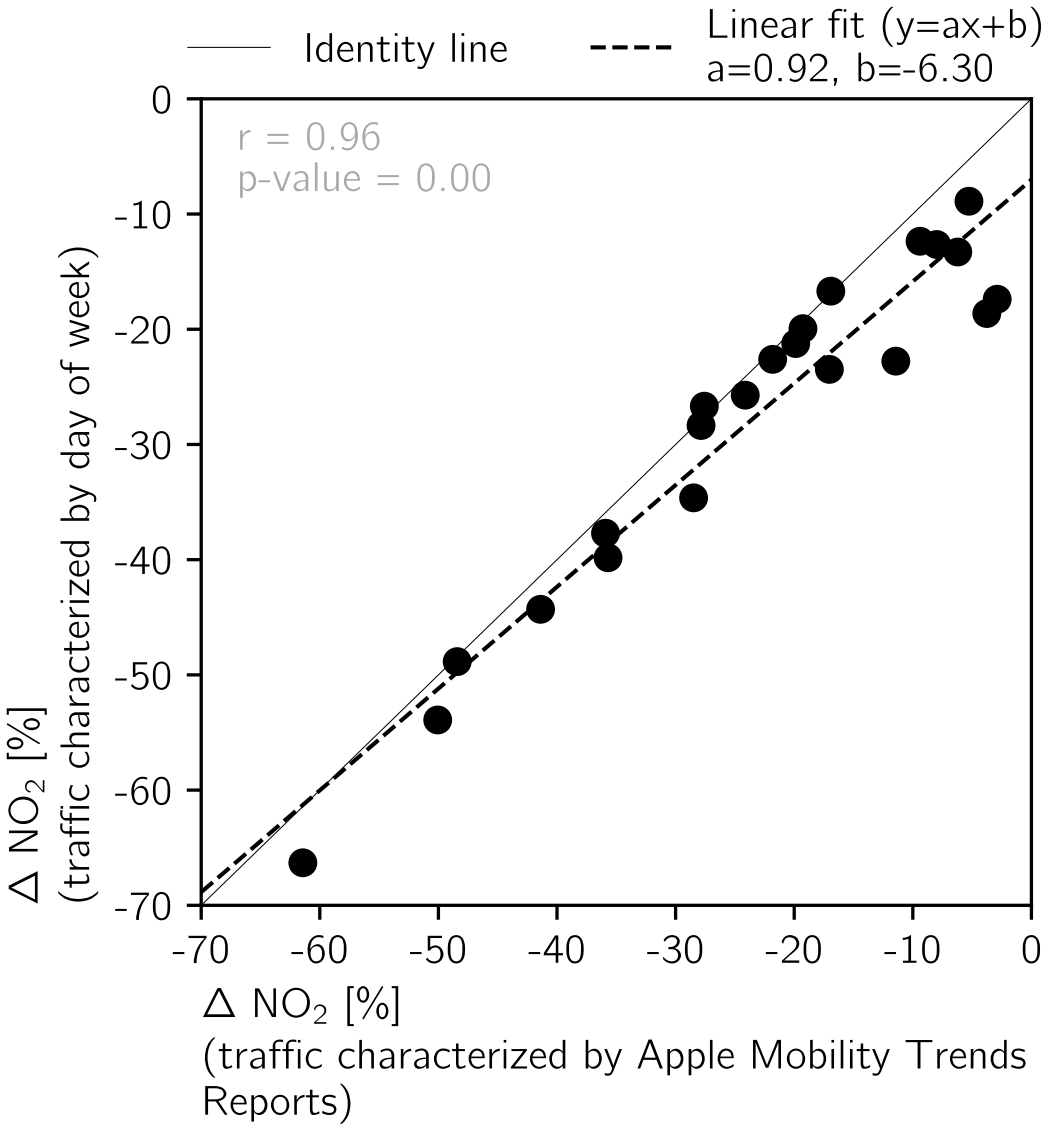

Figure S8. Comparison of ΔNO_2 determined by replacing daily traffic volume with integers corresponding to the day of the week versus ΔNO_2 determined with Apple Mobility Trends Reports. Each point corresponds to a different focus city. The plot's legend indicates the form and coefficients of the linear regression used to describe the relationship between ΔNO_2 from the two different data sources, and inset text shows the correlation coefficient and p-value.

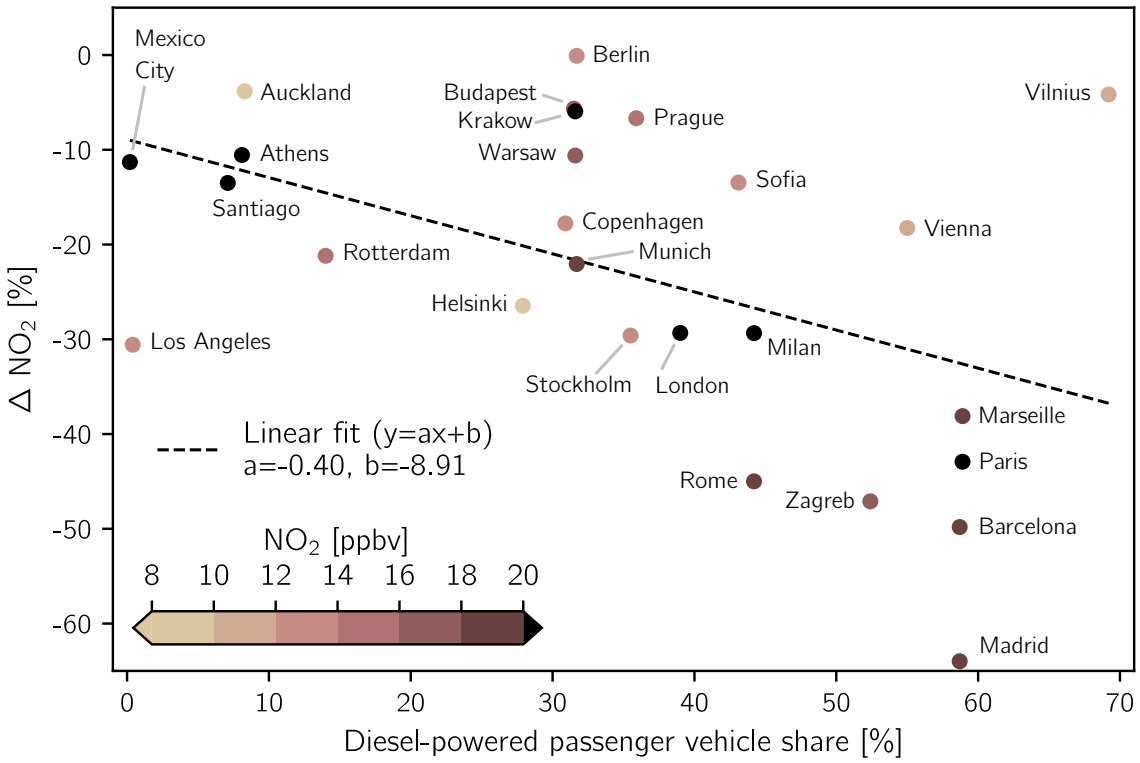

Figure S9. Same as Figure 3 in the main text but ΔNO_2 is calculated over 15 March 2020 - 15 June 2020 for all cities rather than using the dates of country-specific stay-at-home measures ($r = -0.47, p = 0.02$).

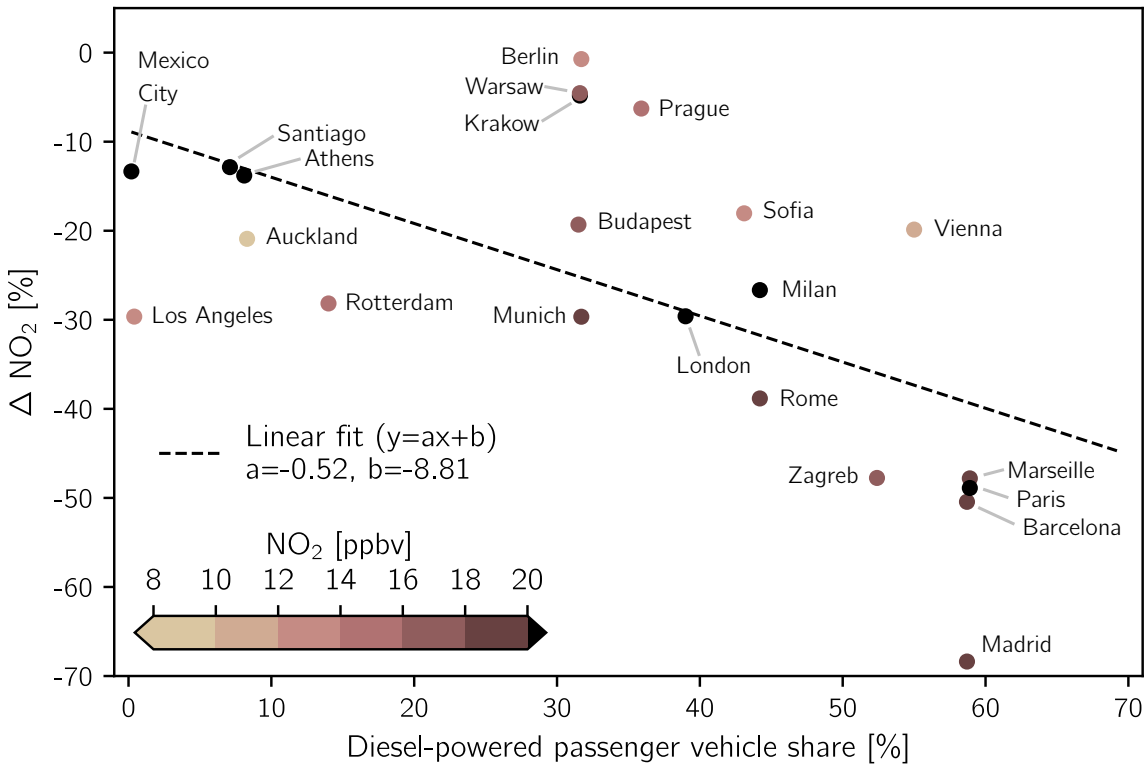

Figure S10. Same as Figure 3 in the main text but ΔNO_2 is calculated only for days with required stay-at-home measures, denoted by the red and maroon colors in Figure S2 ($r = -0.58; p < 0.01$). Copenhagen, Helsinki, Stockholm, and Vilnius did not have required measures (Figure S2) and are thus not included in this figure.

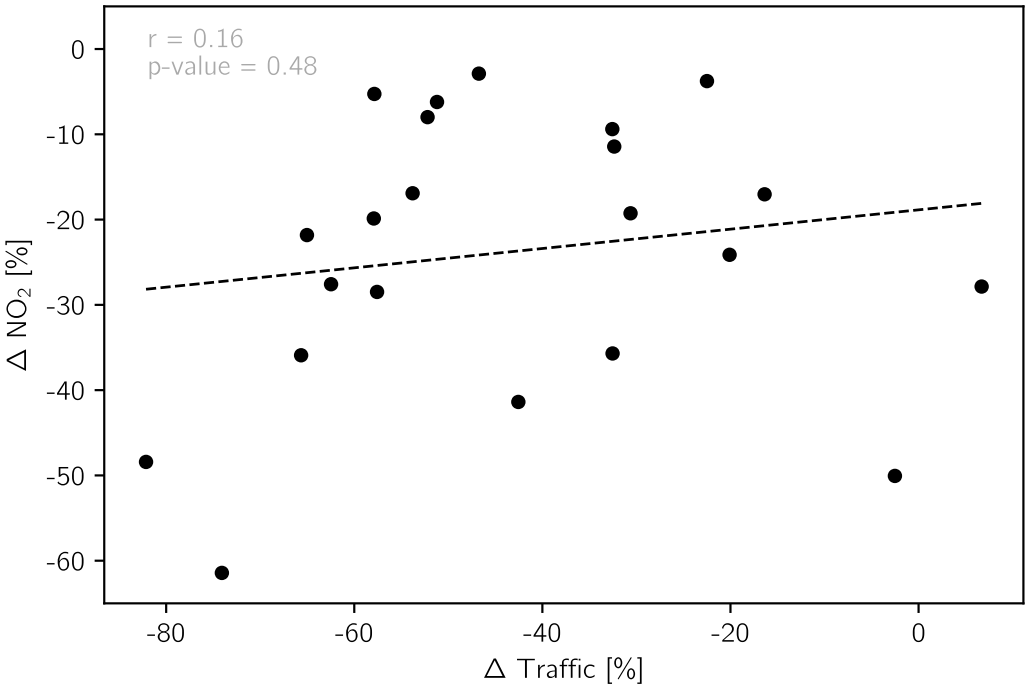

Figure S11. Association of change in traffic with ΔNO_2 for focus cities. Both ΔNO_2 and ΔTraffic are averaged over days with country-specific recommended or required stay-at-home measures. Each point corresponds to a different focus city. The plot's legend indicates the form and coefficients of the linear regression used to describe the relationship between ΔNO_2 and ΔTraffic, and inset text shows the correlation coefficient and p-value.

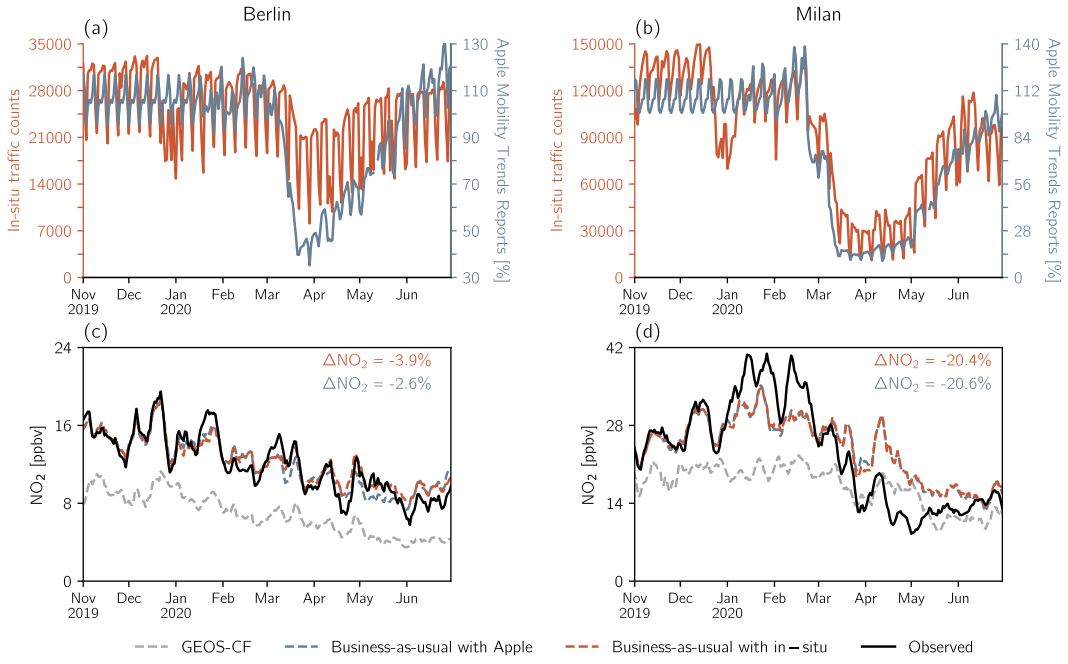

Figure S12. Comparison of traffic trends and business-as-usual NO_2 in Berlin and Milan using different traffic datasets. (a)-(b) Traffic trends from *in-situ* traffic counters and Apple Mobility Trends Reports. (c)-(d) GEOS-CF, observed, and business-as-usual NO_2 concentrations calculated with the different traffic datasets. Text in the upper right corners of (c)-(d) indicates ΔNO_2 determined using the two different input traffic datasets.

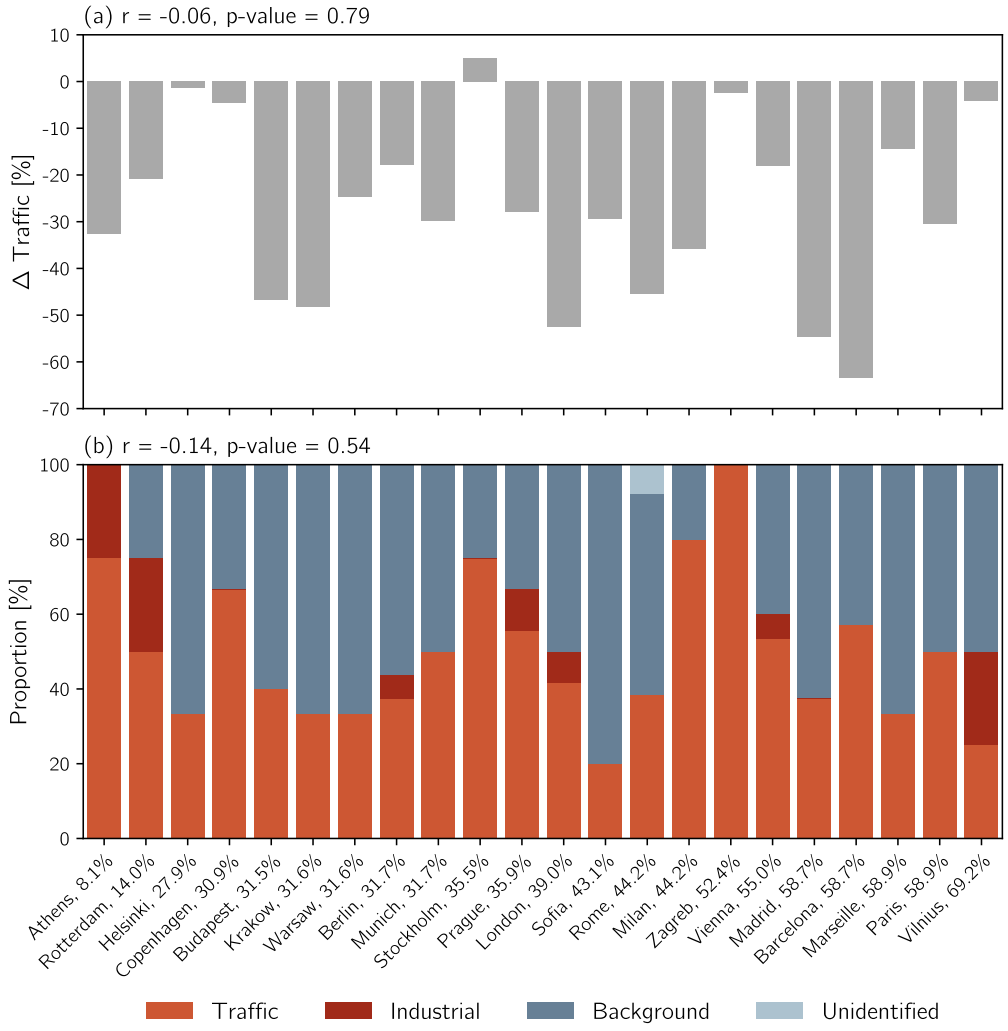

Figure S13. (a) Mobility restrictions, characterized by the average change in traffic volumes during lockdowns relative to the baseline volumes, in each city and (b) proportion of land-use type at *in-situ* NO_2 monitors in each city. Cities are ordered from smallest to largest diesel shares, and each share is indicated alongside city names on the horizontal axis. The correlation coefficient and p-value of (a) mobility restrictions and (b) the number of traffic monitors with diesel shares is shown above each plot. Land-use types in (b) are designated by the European Environment Agency.

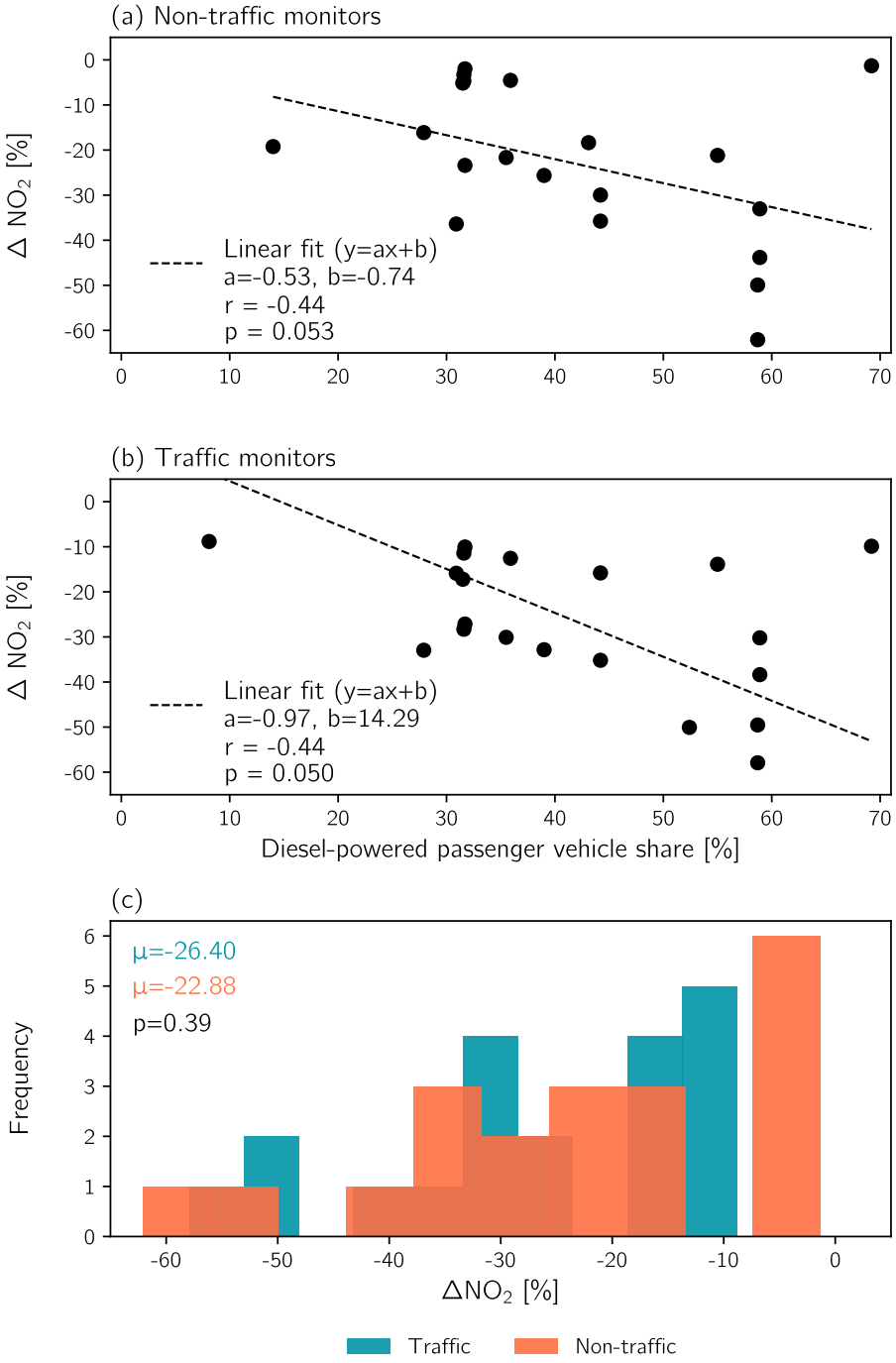

Figure S14. Interpretation of (a)-(b) follows Figure 3 in the main text, but ΔNO_2 was calculated using (a) non-traffic and (b) NO_2 monitors. Here, non-traffic monitors correspond to monitors sited in industrial, background, or unknown environments, designated by the European Environment Agency. (c) shows the distributions of ΔNO_2 for different monitor types. Colored text indicates mean values for each distribution, and the p-value, assessing whether differences between these distributions are statistically significant, is determined with the Kolmogorov-Smirnov test statistic.

References

[1] Agency EE. Air Quality e-Reporting (AQ e-Reporting); 2018. Available from: https://www.eea.europa.eu/data-and-maps/data/aqereporting-8.

[2] Diaz S, Mock P, Bernard Y, Bieker G, Pniewska I, Ragon PL, et al.. European vehicle market statistics 2020/21; 2020. Accessed April 14, 2021. https://theicct.org/publications/european-vehicle-market-statistics-202021.

[3] Association EAM. ACEA Report Vehicles in use Europe, January 2021; 2021. Accessed April 14, 2021. https://www.acea.auto/publication/report-vehicles-in-use-europe-january-2021/.

[4] Liu J, Lipsitt J, Jerrett M, Zhu Y. Decreases in Near-Road NO and NO2 Concentrations during the COVID-19 Pandemic in California. Environmental Science & Technology Letters. 2020;8(2):161-7. Available from: https://doi.org/10.1021/acs.estlett.0c00815.

[5] Kerr GH, Goldberg DL, Anenberg SC. COVID-19 pandemic reveals persistent disparities in nitrogen dioxide pollution. Proceedings of the National Academy of Sciences. 2021 Jul;118(30):e2022409118. Available from: https://doi.org/10.1073/pnas.2022409118.

[6] Apple. COVID-19 Mobility Trends Reports; 2020. Available from: https://covid19.apple.com/mobility.

[7] Cot C, Cacciapaglia G, Sannino F. Mining Google and Apple mobility data: temporal anatomy for COVID-19 social distancing. Scientific Reports. 2021 Feb;11(1). Available from: https://doi.org/10.1038/s41598-021-83441-4.

[8] Venter ZS, Aunan K, Chowdhury S, Lelieveld J. COVID-19 lockdowns cause global air pollution declines. Proceedings of the National Academy of Sciences. 2020 Jul;117(32):18984-90. Available from: https://doi.org/10.1073/pnas.2006853117.

[9] Hale T, Angrist N, Goldszmidt R, Kira B, Petherick A, Phillips T, et al. A global panel database of pandemic policies (Oxford COVID-19 Government Response Tracker). Nature Human Behaviour. 2021 Mar;5(4):529-38. Available from: https://doi.org/10.1038/s41562-021-01079-8.

[10] Keller CA, Knowland KE, Duncan BN, Liu J, Anderson DC, Das S, et al. Description of the NASA GEOS Composition Forecast Modeling System GEOS-CF v1.0. Journal of Advances in Modeling Earth Systems. 2021 Apr;13(4). Available from: https://doi.org/10.1029/2020ms002413.

[11] Bey I, Jacob DJ, Yantosca RM, Logan JA, Field BD, Fiore AM, et al. Global modeling of tropospheric chemistry with assimilated meteorology: Model description and evaluation. Journal of Geophysical Research: Atmospheres. 2001 Oct;106(D19):23073-95. Available from: https://doi.org/10.1029/2001jd000807.

[12] Keller CA, Long MS, Yantosca RM, Silva AMD, Pawson S, Jacob DJ. HEMCO v1.0: a versatile, ESMF-compliant component for calculating emissions in atmospheric models. Geoscientific Model Development. 2014 Jul;7(4):1409-17. Available from: https://doi.org/10.5194/gmd-7-1409-2014.

[13] Long MS, Yantosca R, Nielsen JE, Keller CA, da Silva A, Sulprizio MP, et al. Development of a grid-independent GEOS-Chem chemical transport model (v9-02) as an atmospheric chemistry module for Earth system models. Geoscientific Model Development. 2015;8(3):595-602. Available from: https://doi.org/10.5194/gmd-8-595-2015.

[14] Hu L, Keller CA, Long MS, Sherwen T, Auer B, Silva AD, et al. Global simulation of tropospheric chemistry at 12.5 km resolution: performance and evaluation of the GEOS-Chem chemical module (v10-1) within the NASA GEOS Earth system model (GEOS-5 ESM). Geoscientific Model Development. 2018 Nov;11(11):4603-20. Available from: https://doi.org/10.5194/gmd-11-4603-2018.

[15] Darmenov AS, Silva AMD. The Quick Fire Emissions Dataset (QFED): Documentation of versions 2.1, 2.2 and 2.4. Greenbelt, MD: NASA Goddard Space Flight Center; 2015. 38 (NASA/TM–2015–104606). Available from: http://gmao.gsfc.nasa.gov/pubs/docs/Darmenov796.pdf.

[16] Janssens-Maenhout G, Crippa M, Guizzardi D, Dentener F, Muntean M, Pouliot G, et al. HTAP_v2.2: a mosaic of regional and global emission grid maps for 2008 and 2010 to study hemispheric transport of air pollution. Atmospheric Chemistry and Physics. 2015 Oct;15(19):11411-32. Available from: https://doi.org/10.5194/acp-15-11411-2015.

[17] Keller CA, Evans MJ, Knowland KE, Hasenkopf CA, Modekurty S, Lucchesi RA, et al. Global impact of COVID-19 restrictions on the surface concentrations of nitrogen dioxide and ozone. Atmospheric Chemistry and Physics. 2021 Mar;21(5):3555-92. Available from: https://doi.org/10.5194/acp-21-3555-2021.

[18] Knowland KE, Keller CA, Lucchesi RA. File Specification for GEOS-CF Products, GMAO Office Note No. 17; 2020. https://gmao.gsfc.nasa.gov/pubs/docs/Knowland1159.pdf.

[19] Amann M, Bertok I, Borken-Kleefeld J, Cofala J, Heyes C, Höglund-Isaksson L, et al. Cost-effective control of air quality and greenhouse gases in Europe: Modeling and policy applications. Environmental Modelling & Software. 2011;26(12):1489-501. Available from: https://doi.org/10.1016/j.envsoft.2011.07.012.

[20] Stohl A, Aamaas B, Amann M, Baker LH, Bellouin N, Berntsen TK, et al. Evaluating the climate and air quality impacts of short-lived pollutants. Atmospheric Chemistry and Physics. 2015 Sep;15(18):10529-66. Available from: https://doi.org/10.5194/acp-15-10529-2015.

[21] Amann M, Borken-Kleefeld J, Cofala J, Heyes C, Hoglund-Isaksson L, Kiesewetter G, et al. Support to the development of the Second Clean Air Outlook.

Austria: International Institute for Applied Systems Analysis (IIASA); 2020. ENV.C.3/FRA/2017/0012.

[22] Ivatt PD, Evans MJ. Improving the prediction of an atmospheric chemistry transport model using gradient-boosted regression trees. Atmospheric Chemistry and Physics. 2020 Jul;20(13):8063-82. Available from: https://doi.org/10.5194/acp-20-8063-2020.

[23] Shapley LS. 17. A Value for n-Person Games. In: Contributions to the Theory of Games (AM-28), Volume II. Princeton University Press; 1953. p. 307-18. Available from: https://doi.org/10.1515/9781400881970-018.

[24] Lundberg S, Lee SI. An unexpected unity among methods for interpreting model predictions; 2016.

[25] Lundberg S, Lee SI. A Unified Approach to Interpreting Model Predictions; 2017.

[26] Kean AJ, Harley RA, Kendall GR. Effects of Vehicle Speed and Engine Load on Motor Vehicle Emissions. Environmental Science & Technology. 2003 Jul;37(17):3739-46. Available from: https://doi.org/10.1021/es0263588.

[27] Chen T, Guestrin C. XGBoost. In: Proceedings of the 22nd ACM SIGKDD International Conference on Knowledge Discovery and Data Mining. ACM; 2016. p. 785-94. Available from: https://doi.org/10.1145/2939672.2939785.